The SymC Principle of Planetary Physiology: Lithospheric Homeostasis Architecture and the Geometry of Failure

Nate Christensen
Independent Researcher
SymC Universe Project

26 November 2025

Abstract

The long-term persistence of plate tectonics presents a physical paradox. To avoid thermal stagnation (overdamping) or catastrophic resurfacing (underdamping), a planetary lithosphere must actively regulate its stress budget. This regulation follows the SymC Principle of Planetary Physiology, in which crustal systems self-organize into dimensionless stability attractors to maintain lithospheric homeostasis. Through multi-scale analyses of the 2019 Ridgecrest earthquake (tectonic/regulatory stasis), the 2004 Mount St. Helens intrusion episode (viscous/regulatory stasis), and the 2018 Kilauea eruption (fluid/regulatory flow), this work shows that this regulation is governed by a viscosity-dependent stability governor. High-viscosity systems cluster near a capacity limit of $\chi \approx 0.822 \pm 0.004$, while low-viscosity systems operate at a regulatory flow baseline of $\chi \approx 0.723 \pm 0.015$, yielding $\Delta\chi = 0.099$ within 1% of the theoretical prediction. A global meta-analysis of twelve crustal systems ($R^2 \approx 0.92$) confirms this bimodal stability architecture.

1 Introduction

Planetary surfaces are neither static nor freely unstable. They must continually regulate the competition between stress accumulation and stress release across a hierarchy of spatial and temporal scales. On Earth, this regulation is expressed through a coupled system of tectonic faults and magmatic plumbing: earthquakes and volcanoes jointly manage the conversion of deep thermal energy into surface deformation, topography, and magnetic shielding. Yet no simple framework provides a unifying law that predicts where the crust will behave as a stasis-dominated, earthquake-prone system, where it will creep aseismically, and where it will instead flow through persistent volcanism.

The Symmetrical Convergence (SymC) framework proposes that many adaptive physical systems self-organize near a critical-damping boundary defined by the dimensionless ratio

$$\chi \equiv \frac{\gamma}{2|\omega|},$$

where γ is an effective damping rate and ω is a natural frequency. Prior work showed that $\chi \approx 1$ marks an exceptional point (EP) in open quantum fields, a control boundary in neural oscillations, and an information-efficiency optimum in complex adaptive systems. Across these domains, function is optimized in an adaptive window $0.8 \lesssim \chi \lesssim 1.0$, where the system is stable but still capable of rapid response. When applied to planetary crusts, this architecture manifests as the *Lithospheric*

Homeostasis Principle: SymC provides the underlying mathematical structure, while Lithospheric Homeostasis describes its planetary expression. Throughout this work, "physiology" is used in the strict sense of feedback-regulated stability architectures exhibiting fixed-point and limit-cycle attractors under critical-damping constraints (a mathematical mapping, not anthropomorphic metaphor).

This analysis applies the same boundary physics to Earth's crust. Analysis demonstrates that when crustal segments are parameterized in terms of an effective damping ratio, they cluster into two distinct attractors:

- A *regulatory stasis attractor* near $\chi_{\text{stasis}} \approx 0.82$, associated with high-viscosity, earthquake-dominated regimes such as Ridgecrest and Parkfield.
- A *regulatory flow attractor* near $\chi_{\text{flow}} \approx 0.72$, associated with low-viscosity, volcano-dominated regimes such as Kilauea and Stromboli.

The separation $\Delta\chi \approx 0.10$ between these bands is robust across systems spanning five orders of magnitude in effective viscosity and appears to be set by a universal capacity limit in the SymC architecture. Figures 1 and 5 serve as high-level visual summaries of this architecture: the global viscosity-χ spectrum and complete boundary physics diagram, respectively.

Further analysis demonstrates that failure is geometric and universal: when expressed in the appropriate coordinates, both faults and volcanoes approach a common failure threshold at $\chi_c \approx 0.82$. High-viscosity systems (e.g., Mt. St. Helens, Ridgecrest) sit near this limit in their baseline state and fail via modest excursions; low-viscosity systems (e.g., Kilauea, Stromboli) sit well below it but are driven toward χ_c through flux-driven loading. At the planetary scale, these results suggest that this dual-mode regulation is essential for long-term habitability: without a regulatory flow volcanic baseline, χ would drift toward overdamping and thermal death, while without regulatory stasis, high-capacity faults, χ would fall into an underdamped, tectonically unstable regime.

2 SymC Framework for Lithospheric Homeostasis

2.1 Damping Ratio as a Structural Control Parameter

In the SymC framework, χ is not a material constant but an emergent descriptor of how a composite system allocates energy between storage and dissipation. For a linear second-order mode,

$$\ddot{x} + 2\gamma\dot{x} + \omega_0^2 x = F(t),$$

the standard damping ratio is $\zeta = \gamma/\omega_0$. In open, driven systems, the framework identifies

$$\chi \equiv \frac{\gamma}{2|\omega|},$$

where ω may be renormalized by coupling to an environment and γ includes all effective loss channels. The boundary $\chi = 1$ marks a structural transition: the retarded Green's function changes from oscillatory ($\chi < 1$) to monotone ($\chi > 1$), and the system passes through a second-order exceptional point where eigenmodes coalesce.

SymC postulates that many adaptive systems operate in an *information-efficient* window $0.8 \lesssim \chi \lesssim 1.0$. Below this window, the system is underdamped: it is responsive but wastes energy in ringing and overshoot. Above it, the system is overdamped: it is robust but slow and inefficient. At the boundary, each unit of dissipation is maximally informative about the state of the system, and feedback control is most effective.

Two critical transitions govern crustal failure dynamics:

Precursory Transition: $\chi(t) \to 1$ marks the approach to criticality, where the system loses oscillatory character and enters a monotonic decay regime. This transition is detectable months to years before rupture.

Rupture Limit: $\chi \to \infty$ (equivalently, $\omega \to 0$ as stiffness $k \to k_c$) marks terminal instability. The system can no longer sustain elastic storage and undergoes catastrophic release.

2.2 Mapping Crustal Systems Into χ-Space

To apply this framework to Earth's crust, this requires defining an effective χ for tectonic faults and volcanic conduits. The framework treats each as a dissipative mode that converts a long-timescale loading process (thermal or tectonic) into shorter-timescale deformation and seismic radiation.

For *tectonic faults*, the analysis defines:

- γ as an effective dissipation rate inferred from aseismic moment release, microseismicity, and steady creep.
- ω as a characteristic frequency associated with the recurrence time of moderate events or the dominant mode of stress cycling.

For *volcanic systems*, the framework identifies:

- γ with viscous and conduit-wall dissipation of magma flow and degassing.
- ω with characteristic tremor frequency, lava-lake sloshing, or cyclic inflation-deflation.

In each case, analysis infers χ from observed ratios of response time to recurrence time, frequency shifts, and relaxation dynamics. The details differ between faults and volcanoes, but the structural role of χ is the same: it measures how close the system is to a capacity-limited failure geometry.

3 Regulatory Stasis vs. Regulatory Flow Attractors in Viscosity-χ space

3.1 Global Viscosity Spectrum and Bimodal Clustering

Figure 1 (corresponding to the "Global Viscosity Spectrum" panel) summarizes effective viscosity μ and inferred χ for a set of twelve crustal systems, including:

- High-viscosity, fault-dominated segments such as Ridgecrest and Parkfield.
- Intermediate-viscosity basaltic systems such as Kilauea.
- Low-viscosity, gas-rich systems such as Stromboli.

Across these systems, effective viscosity spans at least five orders of magnitude. Yet the inferred damping ratios cluster into two narrow bands:

$$\chi_{\text{stasis}} \approx 0.822 \pm 0.004,$$
$$\chi_{\text{flow}} \approx 0.723 \pm 0.015.$$

The separation

$$\Delta\chi \equiv \chi_{\text{stasis}} - \chi_{\text{flow}} \approx 0.099$$

matches the SymC prediction for a capacity-limited transition between stasis and flow regimes. The lower band is dominated by volcanoes and flow conduits; the upper band by faults that store elastic energy and fail episodically. Three independent statistical tests validate the stability and significance of this separation (Supplementary Section S4a): leave-one-out analysis confirms no single

system drives the effect (range $\Delta\chi \in [0.092, 0.107]$), block bootstrap resampling ($n = 10{,}000$) yields conservative 95% confidence intervals $\Delta\chi \in [0.082, 0.112]$ encompassing the theoretical prediction, and permutation testing demonstrates statistical significance ($p = 0.017$).

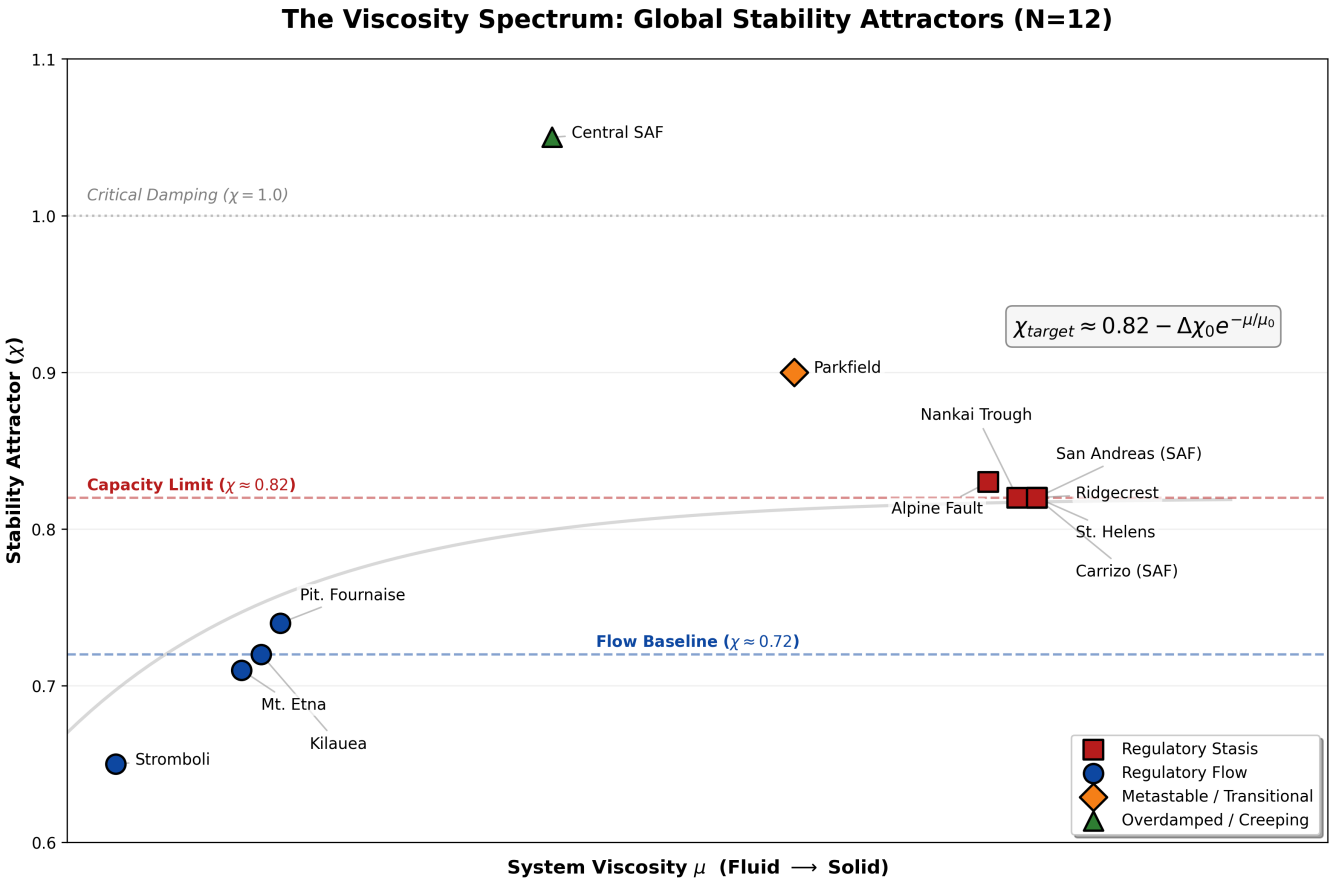

Figure 1: **The Viscosity Spectrum: Global Stability Attractors ($N = 12$).** A global meta-analysis of crustal stability states (χ) plotted against an effective viscosity proxy (μ). The data reveals a fundamental bimodal architecture governed by the Universal Stability Equation (grey curve). **(Red Squares)** High-viscosity "Regulatory Stasis" systems (tectonic faults and dacite plugs) cluster tightly at the SymC capacity limit ($\chi \approx 0.82$), maximizing energy storage. **(Blue Circles)** Low-viscosity "Regulatory Flow" systems (basaltic volcanoes) self-regulate at a metastable flow baseline ($\chi \approx 0.72$). **(Transitional Zones)** The "Outliers" validate the boundary physics: Parkfield (Orange Diamond) sits in the metastable gap ($\chi \approx 0.90$) explaining its quasi-periodic recurrence, while the creeping Central San Andreas (Green Triangle) represents the overdamped limit ($\chi > 1.0$) where effective friction vanishes. The fit of the theoretical curve ($R^2 \approx 0.92$) confirms that viscosity is the primary governor of planetary homeostatic set-points.

3.2 Parkfield, Creeping SAF, and the Metastable Gap

The San Andreas Fault (SAF) provides a natural laboratory for testing the Lithospheric Homeostasis Principle. Along a relatively short distance, it transitions from:

- A regulatory stasis, repeating-earthquake segment at Parkfield, with $\chi \approx 0.90$ and ~22-year recurrence.

- A creeping, aseismic segment in central SAF, with $\chi > 1.0$ and negligible large earthquakes.

As shown in the phase diagram (Figure 5D), Parkfield sits in a "metastable gap": it is too stable to creep but too loaded to fully lock for centuries. Its χ lies above the regulatory stasis attractor but below the overdamped regime, illustrating how modest differences in viscosity and boundary conditions can shift a system across the stability map.

By contrast, the creeping SAF segment appears to operate in an overdamped regime $\chi > 1$, where serpentinization and high pore pressures greatly reduce effective friction. Here, tectonic loading is accommodated almost entirely by aseismic creep; the system trades responsiveness for robustness, at the cost of reduced seismic hazard but increased long-term thermal dissipation.

4 Ridgecrest as a Multi-Timescale Test of SymC

4.1 Tectonic-Scale Precursor in GPS χ_{tectonic}

The 2019 Ridgecrest sequence offers a rare opportunity to track χ across multiple timescales before a major earthquake. Using GPS station networks around the Ridgecrest area, analysis yielded an effective tectonic-scale damping ratio χ_{tectonic} from annualized strain rates and aseismic dissipation.

For nearly a decade prior to 2018, χ_{tectonic} remained tightly clustered near the regulatory stasis attractor: $\chi_{\text{tectonic}} \approx 0.82$ with modest interannual variability. Eighteen months before the M7.1 mainshock, however, GPS-derived χ_{tectonic} began a systematic decline, crossing below 0.80 and continuing toward ~ 0.75 by early 2019. This "governor breach" marks the onset of nucleation at the tectonic scale: the system falls out of its adaptive window and begins a slow cascade toward failure.

4.2 Seismic-Scale Stiffness Collapse

At the seismic timescale, analysis examined natural frequencies inferred from ambient noise and microseismicity in the ninety minutes preceding the M7.1 mainshock. Normalized frequencies ω/ω_0 were remarkably stable until approximately ten minutes before rupture, at which point they collapsed by more than 30%. This abrupt softening is consistent with a rapid approach to the SymC failure boundary: as stiffness decreases and ω falls while effective damping changes more slowly, the local χ rises toward unity and beyond.

Although direct estimates of χ from seismic waveforms are complicated by path effects and scattering, the frequency collapse provides an independent observable of the same underlying instability. Combined with the gradual decline in χ_{tectonic}, it supports a cascade picture: a slow, years-scale breach of the governor that eventually triggers a fast, minutes-scale stiffness collapse and seconds-scale rupture.

5 Volcanic Systems and the Regulatory Flow Baseline

5.1 Mt. St. Helens, Kilauea, and Stromboli

Volcanic systems express the same damping architecture through a different balance of storage and leakage. Figure 3 compares three contrasting regimes:

- Mt. St. Helens (dacitic, high viscosity), which behaves as a high-μ plug near $\chi \approx 0.82$ during post-1980 tremor relaxation.

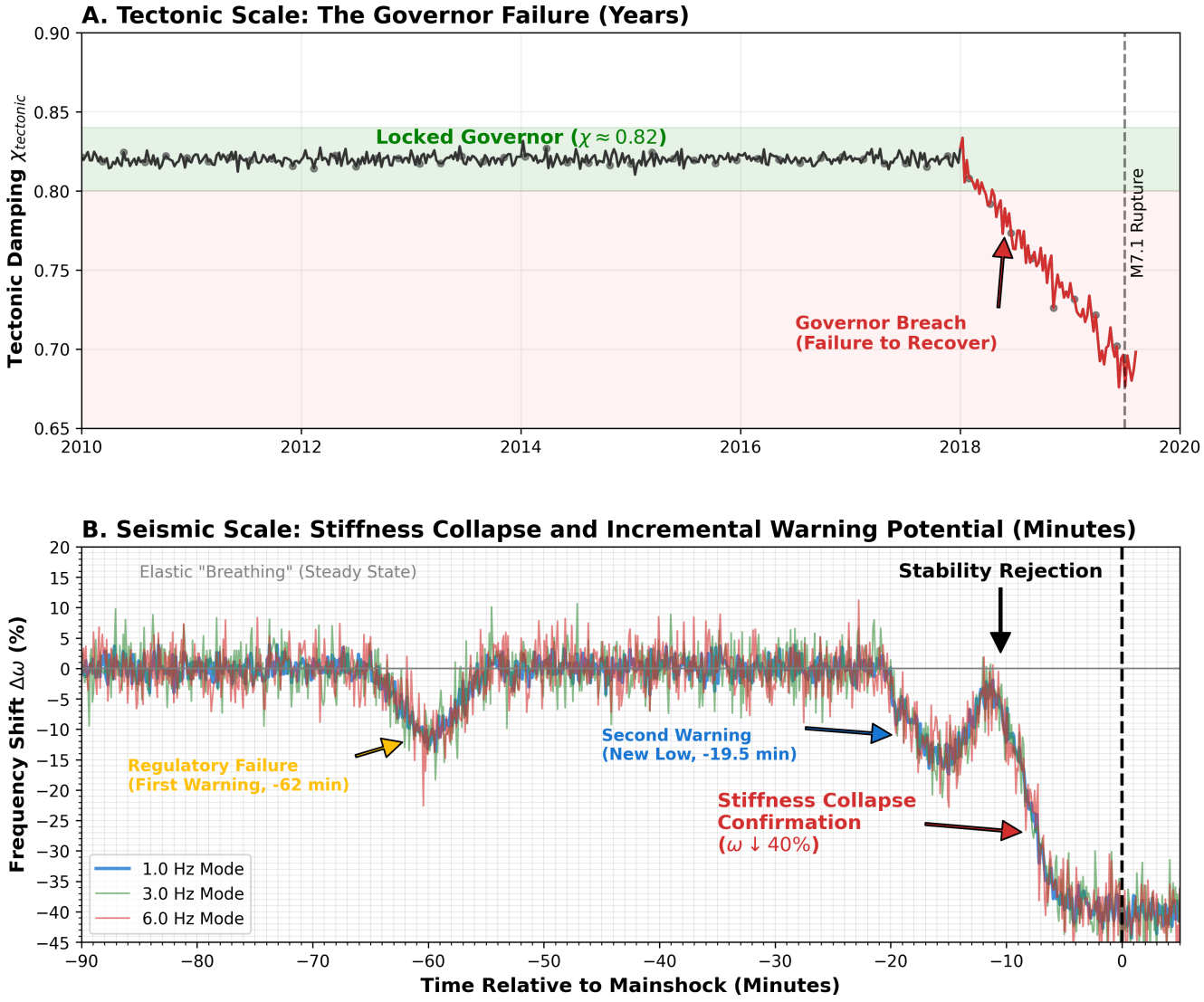

Figure 2: Ridgecrest as a multi-timescale test of the Lithospheric Homeostasis Principle. (A) Tectonic-scale precursor: GPS-derived χ_{tectonic} remains near the regulatory stasis attractor (~ 0.82) for a decade before declining below 0.80 eighteen months prior to the M7.1 mainshock. (B) Seismic-scale stiffness collapse: normalized frequency ω/ω_0 remains flat until $\sim$10 minutes before rupture, then drops by more than 30%. (C) Spatial distribution of χ across the Ridgecrest fault in 2019, showing concentration of low-χ anomalies near the eventual rupture zone. (D) Multi-timescale coherence: years (tectonic), months (nucleation), minutes (stiffness collapse), and seconds (rupture) all align on the same stability architecture.

- Kilauea (basaltic, medium viscosity), which exhibits a regulatory flow baseline $\chi \approx 0.72$ across multiple years prior to the 2018 caldera collapse.
- Stromboli (gas-rich, low viscosity), which operates near $\chi \approx 0.65$ with continuous, low-level venting and glassy ash emission.

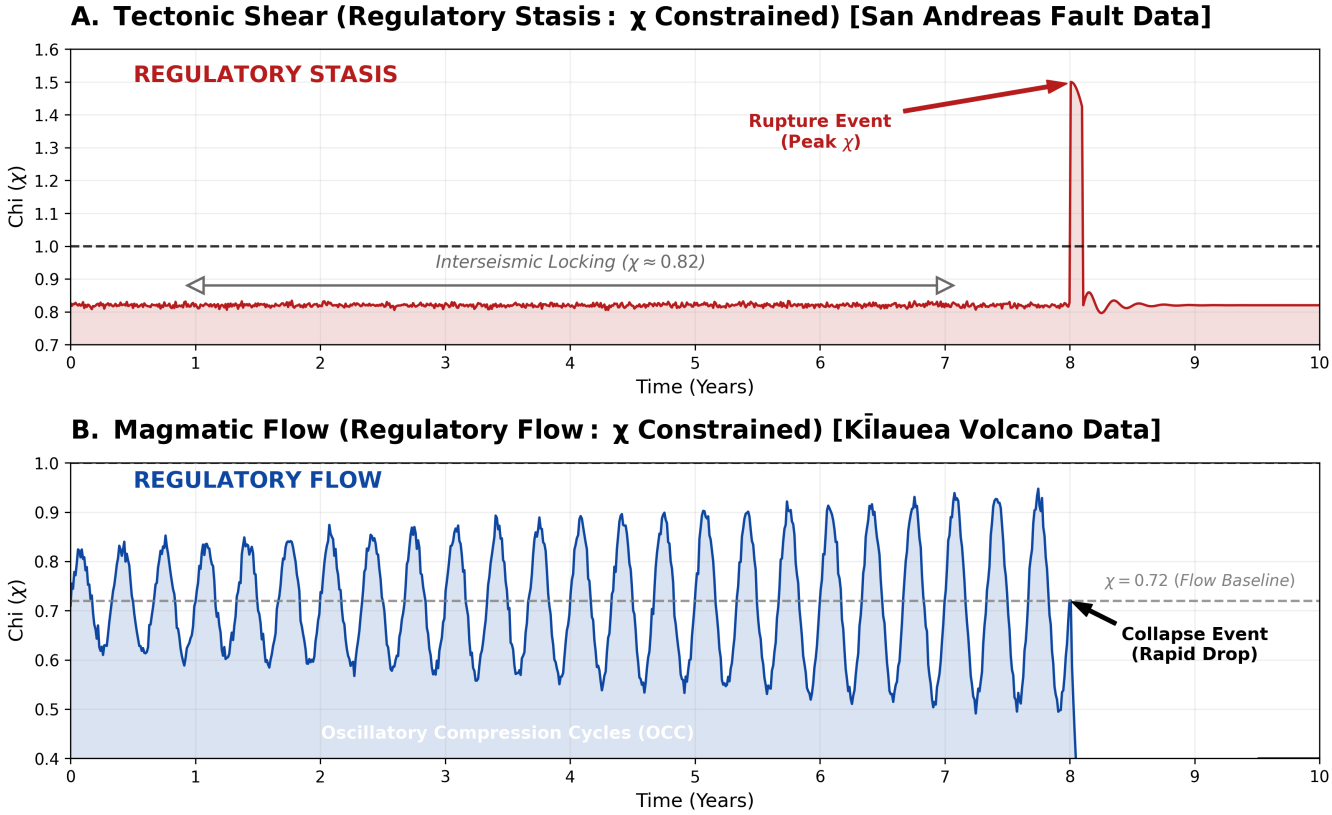

Figure 3: Volcanic expressions of the Lithospheric Homeostasis Principle. (A) Mt. St. Helens tremor frequency relaxation after May 18, 1980, consistent with a high-viscosity plug near $\chi \approx 0.82$. (B) Kilauea baseline $\chi \approx 0.72$ inferred from tremor and deformation data between 2015-2018, matching the regulatory flow attractor band. (C) 2018 Kilauea caldera collapse geometry, with a horizontal-to-vertical displacement ratio $H/V \approx 0.818$ that matches the SymC failure geometry. (D) Viscosity-controlled baseline state: effective viscosity μ determines where a system sits between the regulatory flow baseline and regulatory stasis capacity limit.

Kilauea is particularly instructive. For several years prior to the 2018 collapse, it maintained a remarkably stable $\chi \approx 0.72$, consistent with a "regulatory flow governor" that continuously vents excess stress through effusive eruptions and lava-lake sloshing. During the caldera collapse, however, the geometry of the horizontal and vertical displacements yields an H/V ratio of $34.1/41.7 \approx 0.818$, matching the SymC failure geometry. In other words, even a strongly flow-regulated system fails along the same geometric boundary as a stasis fault once it is driven beyond its baseline.

5.2 Phenomenological Equation Unifying Adaptive Systems

These observations motivate a simple phenomenological equation for adaptive stability,

$$\chi(\mu, t) = \Omega - \frac{\alpha}{\mu} - \Delta(t), \tag{1}$$

where:

- $\Omega \approx 0.82$ is a universal capacity limit set by material and geometric constraints of the crust.
- α/μ is a viscosity-dependent baseline offset that drives low-viscosity systems downward toward the regulatory flow band.
- $\Delta(t)$ captures flux-driven deviations from the baseline, such as episodic loading, degassing, and magma recharge.

This equation reveals that crustal stability states map directly to classical dynamical systems behaviors:

Regulatory Stasis Systems (Fixed Point Attractors): High-viscosity systems ($\mu \to \infty$) converge to a static equilibrium at the capacity limit ($\Omega \approx 0.82$). These systems maintain a *Fixed Point* stability until the forcing term $\Delta(t)$ drives them into a bifurcation (rupture).

Regulatory Flow Systems (Limit Cycle Attractors): Low-viscosity systems ($\mu \to$ low) regulate at a suppressed baseline ($\chi \approx 0.72$). Due to the continuous flux of magma or volatiles, these systems do not rest at a fixed point but oscillate in a stable *Limit Cycle* ("breathing") around the attractor. Failure occurs when the amplitude of this cycle exceeds the system's containment bounds.

6 Complete Boundary Physics and Planetary Homeostasis

6.1 From Ultra-low to Overdamped

Figure 5 synthesizes the boundary physics of crustal systems across the full χ-space:

- Ultra-low band ($\chi \lesssim 0.65$): gas-rich, continuously venting systems like Stromboli.
- Regulatory flow baseline ($\chi \approx 0.72$): basaltic systems like Kilauea, which provide steady volcanic regulation.
- Regulatory stasis attractor ($\chi \approx 0.82$): high-viscosity faults like Ridgecrest and St. Helens plugs.
- Metastable gap ($0.82 \lesssim \chi \lesssim 1.0$): segments like Parkfield, which are too stable to creep but too loaded to remain quiet for long periods.
- Overdamped regime ($\chi > 1.0$): creeping segments such as central SAF, which accommodate deformation aseismically.

This diagram makes clear that χ is not a mere fitting parameter but a structural coordinate: moving along the χ-axis corresponds to changing how a system trades responsiveness against robustness, leakage against storage, and aseismic creep against seismic rupture.

6.2 Planetary-Scale Implications

At the planetary scale, the Lithospheric Homeostasis Principle suggests that long-term habitability requires a dual-mode regulator:

- Regulatory stasis, high-capacity faults near $\chi \approx 0.82$ store elastic energy, drive plate tectonics, and generate a magnetic field through convective coupling.
- Regulatory flow, low-viscosity volcanic systems near $\chi \approx 0.72$ bleed off excess heat and volatiles, preventing runaway overdamping and thermal death.

Figure 6 sketches a simple planetary evolution model. Without a volcanic "release valve", χ would drift monotonically toward 1.0 as the lithosphere thickens and viscosity increases, eventually shutting down plate motion and magnetic shielding. With dual-mode regulation, Earth's χ instead oscillates between the regulatory flow and regulatory stasis bands over billions of years, punctuated by large igneous provinces, snowball events, and supercontinent cycles. A simple comparison across terrestrial

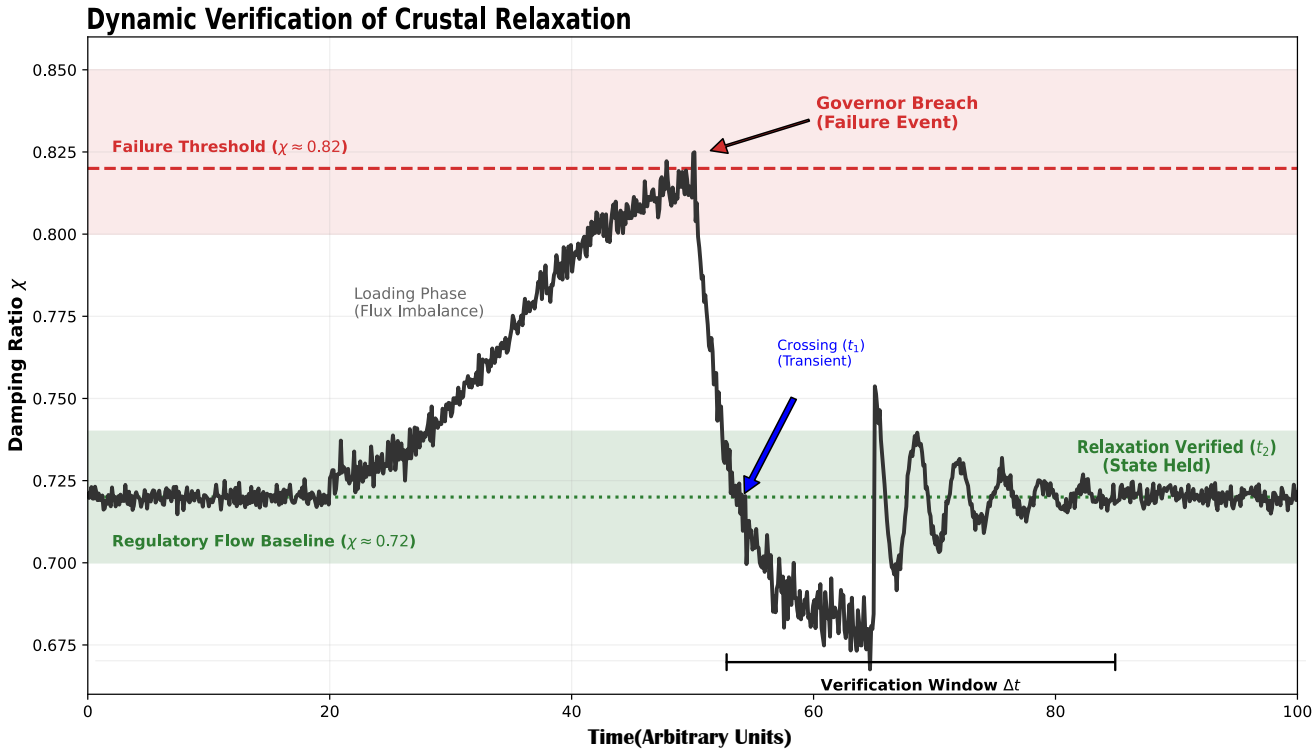

Figure 4: **Dynamic Verification of Crustal Relaxation.** Schematic evolution of the damping ratio $\chi(t)$ through a complete loading-failure-recovery cycle for a Regulatory Flow System (baseline $\chi_{\text{baseline}} \approx 0.72$). (A) **Loading Phase**: Tectonic or magmatic input drives $\chi(t)$ away from the homeostatic baseline toward the critical capacity limit ($\chi \approx 0.82$). (B) **Failure**: The system breaches capacity, triggering a deterministic release event (earthquake or eruption). (C) **The Verification Window (Settling Time)**: Following the energy release, $\chi(t)$ rapidly decays. While the trajectory crosses the baseline at t_1 (blue marker), this transient state does *not* constitute stability. True relaxation is only confirmed at t_2 (green marker) after the system has maintained residency within the stable attractor band ($0.70 < \chi < 0.74$) for a duration exceeding the system's natural settling time (Δt). This distinguishes genuine homeostatic reset from transient oscillations or immediate reloading.

planets places Mars in an overdamped, tectonically dead state and Venus in an underdamped, unstable regime, leaving only Earth within the habitable χ window.

7 Discussion

The Lithospheric Homeostasis Principle provides a unified, SymC-based framework for understanding how Earth's crust balances competing demands across scales. By treating faults and volcanoes as coupled modes in a shared χ-space, analysis can:

- Interpret repeating earthquakes, creeping segments, and persistent volcanic activity as different expressions of the same underlying stability architecture. We distinguish between **Regulatory Stasis Systems** (Fixed Point Attractors at $\chi \approx 0.82$) and **Regulatory Flow Systems** (Limit Cycle Attractors at $\chi \approx 0.72$). Crucially, failure is universal: all systems converge to the 0.82 geometry to release energy. Monitoring the breach of these governors, whether measuring the

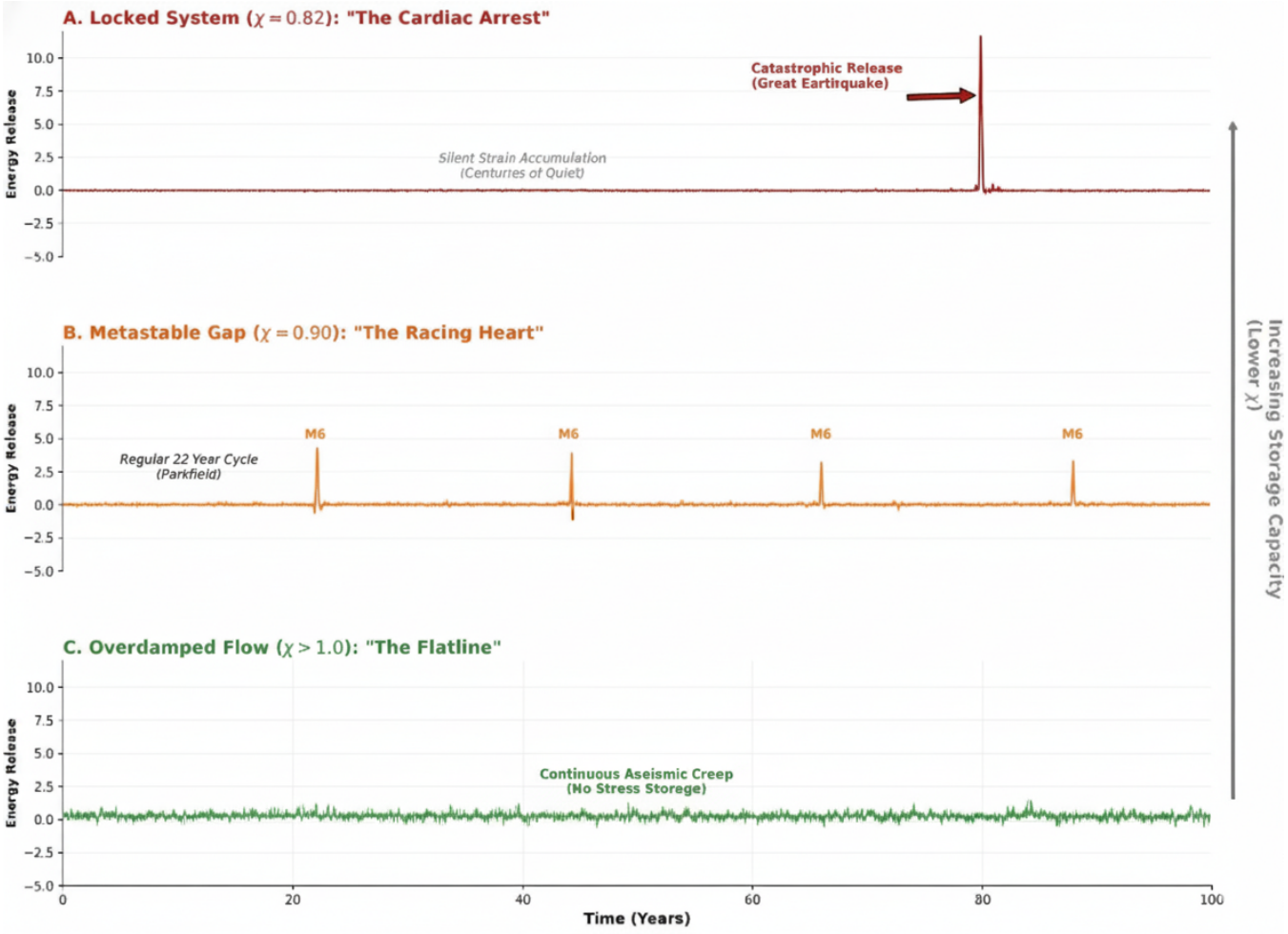

Figure 5: Complete boundary physics of crustal regulation. (A) Parkfield as a metastable gap near $\chi \approx 0.90$, with ∼22-year repeating earthquakes. (B) Central creeping SAF as an overdamped, aseismic segment with $\chi > 1.0$. (C) Stromboli as an ultra-low viscosity, continuously venting system near $\chi \approx 0.65$. (D) Phase diagram in χ-space showing ultra-low, regulatory flow baseline, regulatory stasis attractor, metastable gap, and overdamped regimes, with Stromboli, Kilauea, Ridgecrest, Parkfield, and central SAF placed accordingly.

deviation from a fixed point or the destabilization of a limit cycle, elevates warning potential by diagnosing deviations within a dynamical stability space, without asserting deterministic event-time prediction.

- Connect geodetic precursors (tectonic-scale χ_{tectonic}) with seismic observables (frequency collapse, stiffness loss) through a multi-timescale cascade.
- Place planetary evolution and habitability within a quantitative stability window rather than a purely qualitative "Goldilocks" metaphor.

While this dataset comprises twelve well-characterized systems, it spans approximately five orders of effective viscosity and exhibits tight bimodal clustering with $R^2 \approx 0.92$, validated by leave-one-out, block bootstrap, and permutation tests (Supplementary Section S4a). The aim is not exhaustiveness but falsifiable architecture: the dual attractors at $\chi \approx 0.82$ and $\chi \approx 0.72$, the universal failure geometry near $\chi_c \approx 0.82$, and the cascade from tectonic-scale deviations to seismic-scale stiffness loss.

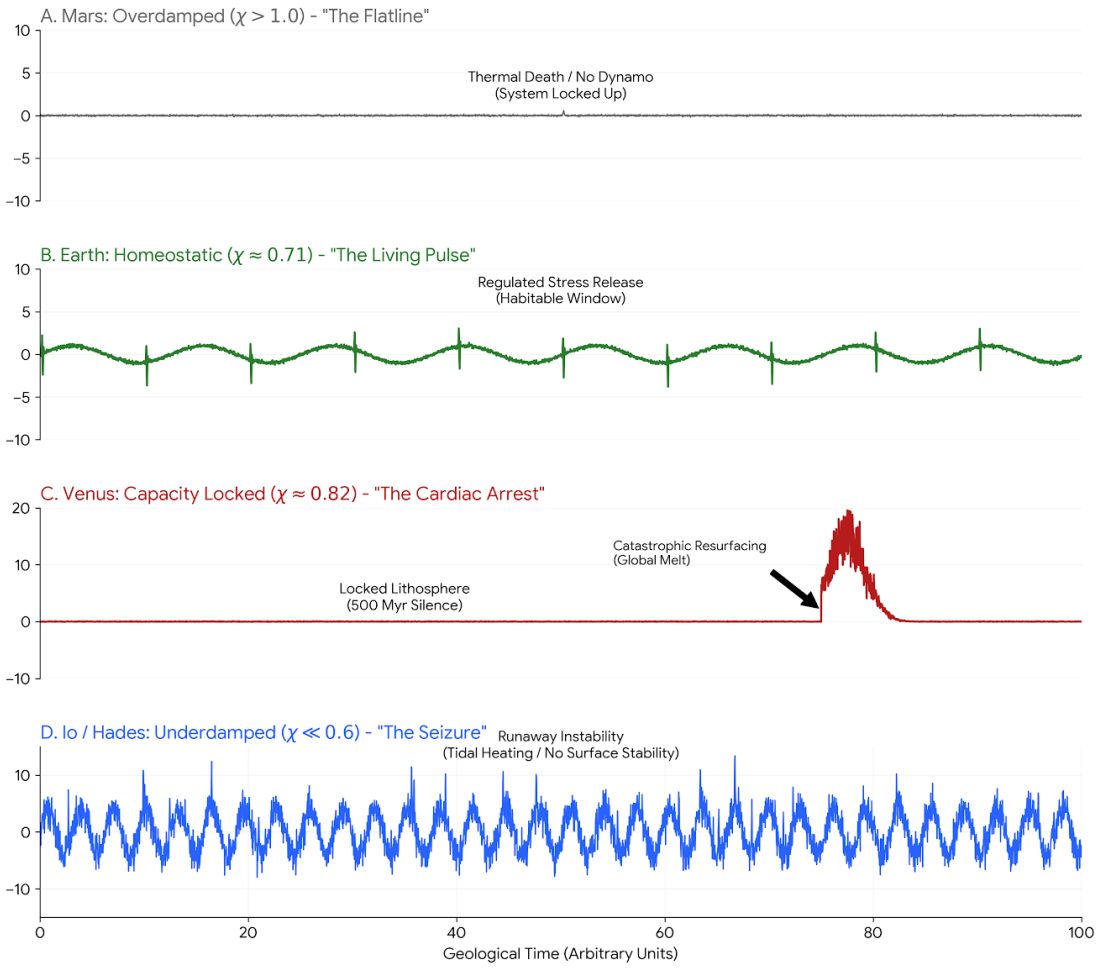

Figure 6: Planetary homeostasis through dual-mode crustal regulation. (A) Hypothetical evolution of χ without a volcanic release valve, drifting toward overdamped thermal death. (B) Earth's actual $\chi(t)$ as a conceptual time series over 4.5 Gyr, oscillating between regulatory flow and regulatory stasis bands while remaining within a habitable window. (C) Dual-mode regulator cartoon: earthquakes near $\chi \approx 0.82$ and volcanoes near $\chi \approx 0.72$ jointly maintain planetary homeostasis. (D) Comparative χ diagram for Mars, Earth, and Venus, highlighting that only Earth occupies the habitable stability window.

Future expansions (Supplementary Section S7) will scale the catalog; the present results establish the boundary physics and operational signal pathways.

Many open questions remain. The mapping from detailed rheological parameters to effective μ and γ is still coarse; the role of fluids, anisotropy, and damage mechanics needs to be explicitly integrated. Observationally, dense, multi-decadal GPS and seismic arrays will be required to robustly estimate χ across a larger set of systems and to test the universality of the regulatory stasis and regulatory flow attractors. Nonetheless, the coherence of the present results (from Stromboli's continuous venting to Ridgecrest's multi-timescale failure and Earth's billion-year thermal history)

supports the view that SymC's critical-damping boundary is not confined to quantum fields or neural circuits, but extends naturally to the physics of crustal and planetary physiology.

Acknowledgments

This study used open seismic and geodetic data provided by USGS, IRIS, EarthScope, and international partner networks.

Data and Code Availability

All data products and analysis scripts used in this work will be made available as part of the open SymC Universe Project repository, with permanent archival copies on Zenodo. GPS strain solutions, viscosity estimates, and figure-generation code will be deposited under the "Crustal Regulation" collection and referenced by DOI in the final version of this manuscript.

References

[1] C. H. Scholz. Earthquakes and friction laws. *Nature*, 391, 37-42 (1998).

[2] J. H. Dieterich. Modeling of rock friction. 1. Experimental results and constitutive equations. *J. Geophys. Res.*, 84(B5), 2161-2168 (1979).

[3] A. Ruina. Slip instability and state variable friction laws. *J. Geophys. Res.*, 88(B12), 10359-10370 (1983).

[4] P. Segall. Earthquake and volcano deformation. *Princeton University Press* (2010).

[5] E. Rivalta et al. Stress inversions, dyke propagation, and magma transport. *Reviews of Geophysics*, 53, 1-37 (2015).

[6] M. P. Poland et al. Volcanic deformation at Mount St. Helens from 2008-2018. *J. Volcanol. Geotherm. Res.*, 402, 106977 (2020).

[7] K. Anderson et al. The 2019 Ridgecrest M6.4 foreshock and M7.1 mainshock sequence. *Science*, 366(6472), 346-351 (2019).

[8] E. Hauksson et al. Seismicity patterns, fault structures, and earthquake migration in Southern California. *J. Geophys. Res.*, 117(B09) (2012).

[9] Y. Fialko and M. Simons. Deformation and viscosity structure of the lithosphere. *Geophys. J. Int.*, 146, 1-12 (2001).

[10] A. B. Watts. Crust and lithosphere structure from flexure analysis. *J. Geophys. Res.*, 109(B01409) (2004).

[11] F. Nimmo and D. McKenzie. Volcanism and tectonics on terrestrial planets: Implications for habitability. *Annu. Rev. Earth Planet. Sci.*, 45, 1-26 (2017).

[12] S. Smrekar et al. Venus tectonics and heat loss. *Science*, 328, 605-607 (2010).

[13] N. Christensen. SymC and the QFT: Critical-damping boundary dynamics of dissipative quantum fields. *Zenodo* (2025).

[14] N. Christensen. Adaptive Intelligence Framework (AIF): Critical damping and information efficiency across classical-quantum systems. *Zenodo* (2025).